The pH Dependence of CD2 Domain 1 Self-Association and ^{15}N Chemical Exchange Broadening Is Correlated with the Anomalous pK_a of Glu41[†]

H. A. Chen,[‡,§] Mark Pfuhl,[‡,||] and Paul C. Driscoll*[,‡,⊥]

Department of Biochemistry and Molecular Biology, University College London, Gower Street, London WC1E 6BT, United Kingdom, Ludwig Institute for Cancer Research, 91 Riding House Street, London W1W 7BS, United Kingdom, and Department of Biochemistry, University of Leicester, University Road, Leicester LE1 7RH, United Kingdom

Received July 12, 2002; Revised Manuscript Received September 30, 2002

ABSTRACT: We have previously shown using ^{15}N nuclear relaxation measurements that the concentration-dependent rotational correlation time and chemical exchange broadening for selected resonances of rat CD2 domain 1 (CD2d1) are consistent with a model of low-affinity self-association of the protein molecules. The exchange broadening data, which at high protein concentrations highlight selected nuclei in the major C′−C−F−G β-sheet face of the immunoglobulin fold, implicate a surface reminiscent of the major lattice contact within crystals of the intact CD2 ectodomain. In a separate study, we have also demonstrated that the β-strand C′ surface-exposed residue Glu41 possesses an anomalously elevated acidity constant (pK_a = 6.7 at a protein concentration of 1.2 mM). Mutagenesis studies showed that the close contact of residue Glu41 with Glu29 (β-strand C) is the primary cause of the high pK_a. However, the measured pK_a of Glu41 also shows a weak dependence on protein concentration, implicating Glu41 in the mechanism of CD2d1 self-association. In the study presented here, we demonstrate a correlation of the pH dependence of the chemical shift and ^{15}N nuclear relaxation parameters measured for wild-type and mutant forms of CD2d1 with pH and the protonation state of Glu41. Self-association of CD2d1 molecules is promoted whenever the side chain charge of residue 41 is neutralized. These observations are consistent with a model for CD2d1 self-association that corresponds to the crystal structure lattice contact where the interatomic distances are consistent with Glu41 being in the protonated state. This study reinforces the conclusion that residue-specific chemical exchange broadening of protein resonances can arise from weak self-association phenomena. In addition, the electrostatic profile of rat CD2 interfacial residues parallels that of the homologous human CD2 in a manner that suggests a rationalization of similar exchange broadening observations.

The analysis of protein hydrodynamic behavior by examination of heteronuclear relaxation measurements (*1*, *2*) is an increasingly routine component of biomolecular NMR[1] investigations. Such measurements are useful not only for assessing the likely signal-to-noise ratio of particular multidimensional NMR experiments but also for providing a residue-by-residue profile of internal mobility that informs the subsequent analysis of solution structure determinations and functional properties. In the simplest form of the commonly adopted framework of the Lipari−Szabo model-free (L−S MF) formalism (*3*, *4*), the overall motion of the molecules is characterized as an isotropic molecular reorientation correlation time (τ_c). Internal motions are parametrized in terms of generalized order parameters (S^2) and internal correlation times (τ_e) for motions on a time scale much faster than overall tumbling, and phenomenological chemical exchange contributions (R_{ex}) for motions on the time scale of the inverse of the chemical shift difference for resonances of the different conformations that are involved (*5*, *6*).

Application of the L−S MF formalism and the interpretation of the output parameters are often straightforward. Complications can arise, however, under a variety circumstances, for example, when the molecule under investigation does not tumble isotropically, perhaps because of the segmental flexibility of connected globular domains (e.g., in modular proteins), or because for nonglobular states the separation of overall and internal motion time scales implied by the L−S MF formalism does not hold. In the latter case, the "extended" L−S MF formalism (*7*) is often adopted which treats internal motions as those occurring on "fast" and "intermediate" time scales, characterized by order parameters S_f^2 and S_s^2 and time constants τ_f and τ_s, respectively. A particular challenge can arise in cases of "excess" transverse relaxation rates. Where these rates cannot

[†] P.C.D. is grateful for support from the Royal Society and the Ludwig Institute for Cancer Research. During this work, M.P. was supported by a long-term postdoctoral EMBO fellowship and is now a Royal Society University Research Fellow.

* To whom correspondence should be addressed. Phone: (44) 20 7679 7035. Fax: (44) 20 7679 7193. E-mail: driscoll@biochem.ucl.ac.uk.

[‡] University College London.

[§] Current address: Department of Biological Sciences, Imperial College of Science, Technology and Medicine, London SW7 2AZ, United Kingdom.

[||] University of Leicester.

[⊥] Ludwig Institute for Cancer Research.

[1] Abbreviations: CD2d1, CD2 domain 1; IgSF, immunoglobulin superfamily; L−S MF, Lipari−Szabo model free; HSQC, heteronuclear single-quantum coherence; NOE, nuclear Overhauser effect; NMR, nuclear magnetic resonance.

10.1021/bi026447x CCC: $22.00
Published on Web 11/15/2002

be rationalized on the basis of a more complex model of molecular rotation by the introduction of anisotropic diffusion, these contributions to R_2 are interpreted as chemical exchange line broadening, denoted R_{ex}. In a number of published examples, R_{ex} phenomena have been ascribed to intermediate-to-slow time scale concerted motions of secondary structure elements (*8*−*12*).

We have been engaged in the study of the structure−function relationship of the T-cell adhesion molecule CD2. We demonstrated by NMR methods that the structure of domain 1 of rat CD2 (CD2d1) is a member of the immunoglobulin superfamily (IgSF) (*13*), and that the CD48 ligand-binding interface (the C′−C−F−G β-sheet face of the V-type immunoglobulin fold) corresponds to the major lattice contact in crystals of the intact rat CD2 ectodomain (*14*, *15*). However, for a long time, we were unable to secure a consistent analysis of the hydrodynamic properties of the CD2d1 molecule by ^{15}N or ^{13}C nuclear relaxation measurements. In the meantime, Wagner and co-workers reported that the structural homologue human CD2d1 provided evidence for extensive exchange broadening that they attributed to pervasive motions of the major β-sheet face of the molecule (*9*). A breakthrough in the analysis of our data for rat CD2d1 came with the serendipitous discovery that the chemical shifts of numerous resonances were exquisitely sensitive to both protein concentration and sample pH in the pH range of 5−7. Subsequent studies have now demonstrated that under strictly controlled pH conditions (pH 6.0) the apparent overall correlation time and major R_{ex} contributions and chemical shifts of selected resonances are strongly dependent on the protein concentration alone. These observations have been interpreted in terms of a low affinity ($K_D \approx$ 3−6 mM) yet structurally specific self-association of the rat CD2 domain 1 molecules (*16*). In a separate study (*17*), we have characterized the acidity constants of all Glu and Asp residues in the protein and discovered that residue Glu41 (β-strand C′) presents an anomalously elevated pK_a as a result of the proximity of the side chain carboxyl group of Glu29 to the neighboring strand (β-strand C). At a protein concentration of 1.2 mM, the pK_a of Glu41 was found to be 6.7, but this value was also found to be weakly dependent on protein concentration (pK_a = 6.4 at 0.1 mM CD2d1). The study presented here combines these and additional results to indicate conclusively that the self-association of wild-type and mutant rat CD2 domain 1 molecules, evidenced by changes in NMR observables and derived hydrodynamic parameters, is correlated with the charge status of residue 41. Moreover, the results of this analysis are readily understood within the context of the model of the self-associated CD2d1 state provided by the major lattice contact in crystals of the rat CD2 ectodomain, which we argue shows the Glu41 residue in the protonated state.

MATERIALS AND METHODS

Sample Preparation. Wild-type and mutant rat CD2d1 protein samples for this study were prepared as described previously (*16*, *18*). If not otherwise noted, spectra were recorded using samples containing 1.2 mM CD2d1 in 20 mM phosphate buffer. pH values were adjusted by adding small amounts of 1 N NaOH or HCl to the final sample. pH values are mean values of the pH measured immediately before and after NMR data acquisition.

NMR Spectroscopy. Spectra were recorded using Varian UnityPlus spectrometers equipped with three RF channels and triple-resonance *Z*-axis pulsed field gradient probes. All ^{15}N nuclear relaxation experiments (500 MHz for ^{1}H) were measured and the data analyzed in the manner described previously (*16*). ^{13}C chemical shifts were measured during titrations at a ^{1}H frequency of 600 MHz using constant-time HSQC experiments (*19*) with a T delay of 13.6 ms. The spectral widths were 10 000 (^{1}H) and 3500 Hz (^{13}C).

All spectra were processed with nmrPipe (*20*). FIDs were multiplied with a Gaussian window function in F_2 with a line broadening of 2.0 Hz and a weighting factor of 0.01. Interferograms in F_1 were first extended by 64 complex points (from 200 measured) by linear prediction using eight coefficients followed by apodization with a sine-squared function shifted by 80° and zero filling to 512 points. Baseline correction was performed in F_1 and F_2 using a second-order polynomial function. Spectra were analyzed with ANSIG version 3.3 (*21*), AZARA (*22*), and XEASY (*23*). All assignments used in this work are as published in ref *18* and can be obtained from the BioMagResBank database (accession number 4109).

Data Analysis. ^{15}N transverse (R_2) and longitudinal (R_1) relaxation rates and $\{^1H\}^{15}N$ cross-relaxation (heteronuclear NOE) data were analyzed according to the Lipari−Szabo model-free formalism (*3*) with its extension to motions on an intermediate time scale (*7*) as described recently (*16*). The pH dependence of ^{13}C and ^{15}N chemical shift variations was analyzed using home-written Mathematica scripts based on the Henderson−Hasselbalch equation. Chemical shift variation as a function of pH was fit to curves corresponding to one or more independent pK_a values as described previously (*17*).

RESULTS

pH Dependence of the Rotational Diffusion Behavior of CD2d1. We assessed the rotational diffusion characteristics of wild-type CD2d1 over the pH range of 2.0−8.5 by performing a series of ^{15}N R_1 and R_2 and $\{^1H\}^{15}N$ NOE measurements at a constant protein concentration (1.2 mM). These data were analyzed using the extended L−S MF formalism to extract estimates of the isotropic rotational correlation time (τ_c) from average R_2/R_1 ratios, and residue-specific parameters that characterize internal motions on different time scales. Over this pH range, the generally excellent dispersion of the ^{1}H resonances of the CD2d1 spectrum is retained with no indication of a loss of stability or partial unfolding of the protein chain. At each titration point, a good fit of the relaxation data to a model of a globular protein undergoing isotropic rotational diffusion was obtained with only a handful of residues being excluded on the grounds of the data being incompatible with an essentially ordered chain (e.g., small or negative heteronuclear NOEs, or large R_{ex} contributions to the measured R_2 relaxation rate). As was noted in previous studies of the concentration dependence of the relaxation parameters for CD2d1 (*16*), no statistically significant evidence was found that warrants the application of an anisotropic rotational diffusion model for rat CD2d1. Therefore, the following description of the hydrodynamic characteristics of rat CD2d1 is cast in terms of an isotropic model for molecular reorientation.

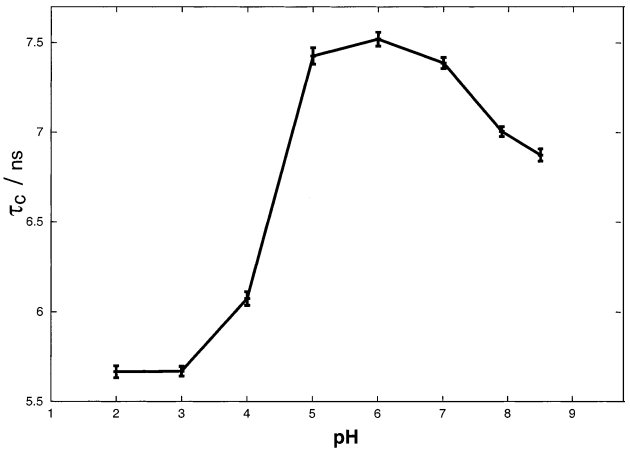

FIGURE 1: Dependence of rotational correlation time of CD2d1 on pH at 25 °C and 1.2 mM protein (^{1}H, 500 MHz).

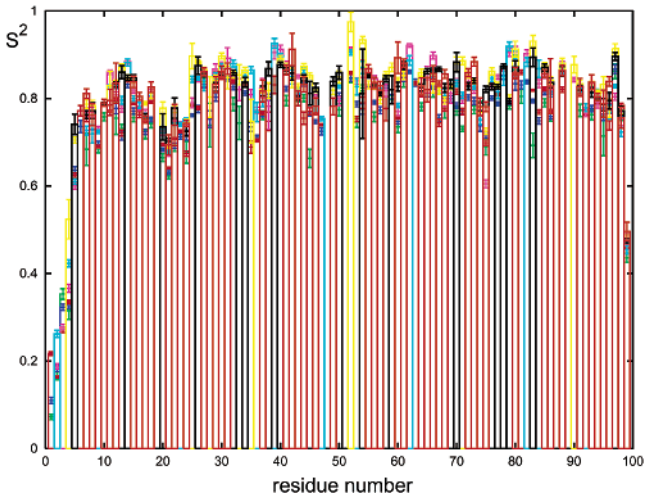

FIGURE 2: Dependence of S^2 for CD2d1 residues as a function of pH at 25 °C (^{1}H, 500 MHz). Colors are yellow for pH 3, red for pH 4, cyan for pH 5, blue for pH 6, black for pH 7, pink for pH 7.9, and green for pH 8.5.

The apparent rotational correlation time of CD2d1 was found to be strongly dependent on the sample pH as shown in Figure 1. A maximum value of τ_c (7.52 ± 0.04 ns) was found at pH 6.0. The derived value of τ_c drops to 5.67 ± 0.04 ns when the pH is decreased to 2.0. The value of τ_c is also diminished (to 6.87 ± 0.03 ns) as the pH is increased from 6.0 to 8.5. Due to the detrimental effects of the base-catalyzed exchange of water with amide protons (leading to a loss of signal intensity), it was not possible to probe the dynamics in a global manner at a pH higher than 8.5.

Residue-Specific Relaxation Parameters. A detailed account of the model-free analysis of the relaxation parameters at pH 6.0 and a protein concentration of 1.2 mM has already been reported (*16*). Therefore, in the following, we focus on pH-dependent variations in the relaxation parameters. Complete lists of all relaxation parameters obtained in this study can be found in the Supporting Information.

For the most part, the derived residue-specific relaxation parameters characteristic of fast internal motions are insensitive to alterations in the sample pH. For the majority of residues, a continuous small increase in the value of S^2 is observed when the pH is increased from 2.0 to 7.0, after which the value remains constant as shown in Figure 2. For a few residues, there is a slight diminution in the value of

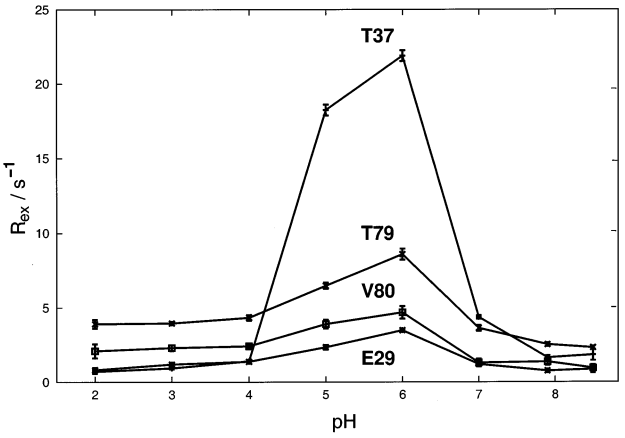

FIGURE 3: Dependence of the phenomenological exchange contribution R_{ex} for the backbone amides of Thr37, Thr79, Val80, and Glu29 on pH at 25 °C and 1.2 mM protein (^{1}H, 500 MHz).

S^2 in the high-pH range. However, the average variation of S^2 over the pH range does not exceed ±0.06 and is only slightly greater than the average statistical uncertainty for S^2. In addition, the general sequence-specific variations of S^2 such as the "dip" in S^2 values around residues Asn20−Asp25 corresponding to the loop connecting β-strands B and C are similar at all pH values.

Residue-specific motional models including dynamics on a fast to intermediate time scale (*7*) were consistently required for only the first eight residues in the protein sequence. For the rest of the chain, intermediate time scale dynamics are only found for pH values around 7.0. The order parameters for the intermediate time scale dynamics are uniformly around 0.8 with the exception of only the first eight residues where S_s^2 drops slightly to 0.6. Only small, nonsystematic variations are seen in the magnitudes of the effective internal motion correlation times that are between 20 and 80 ps for the fast motions (τ_f) and between 0.5 and 3.5 ns for the fast to intermediate time scale motions (τ_s) for the whole range of the titration.

Among all the residue-specific relaxation parameters, the most striking effect of pH is seen for the phenomenological exchange contribution to R_2, R_{ex} (see Figure 3). For a small number of residues, a significant variation is seen across the pH range. Most notable is Thr37 which possesses an R_{ex} of 22 s^{-1} between pH 5.0 and 6.0, which drops to ≈2 s^{-1} toward both pH 2.0 and pH 8.0. R_{ex} variations following the same overall pattern were observed for residues clustered in the Glu29−Ala40 (β-strand C−C′) and Thr79−Thr86 (β-strand F) regions of the polypeptide chain. In contrast, a few residues, e.g. Ile88, show significant but smaller exchange broadening (≈3 s^{-1}) that is essentially independent of pH. For all other residues, R_{ex} was found to be less than 1.5 s^{-1} and essentially independent of pH.

The variation in τ_c and R_{ex} terms with pH indicates that at minimum two transitions in hydrodynamic behavior exist across the pH range that was examined. We have previously interpreted the concentration dependence of τ_c at a constant pH of 6.0 in terms of a self-association CD2d1 monomer−dimer equilibrium. We now propose that the pH dependence of the relaxation parameters is a reflection of variation in the magnitude of the CD2d1 homodimer dissociation constant, K_D. At the low-pH and high-pH extrema of the titration, the association of the CD2d1 monomers is weaker than at

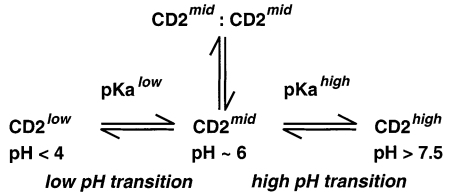

FIGURE 4: Schematic representation of the proposed solution equilibria between the different charge states of rat CD2d1 that are required to rationalize the derived hydrodynamic and exchange contributions to the ^{15}N relaxation rates.

the middling pH value of 5.5. To rationalize this pattern of behavior, we require the CD2d1 molecules to adopt a minimum of three separate states that we will denote here (for simplicity) the low-pH state, CD2d1^{low} (for behavior below pH ≈4); the middle-pH state, CD2d1^{mid} (for behavior at pH ≈6.0); and the high-pH state, CD2d1^{high} (for behavior above pH ≈7.5). It is the middle-pH state that is characterized by enhanced self-association and an elevated value of R_{ex} terms (see Figure 4).

Therefore, elucidation of the molecular identity of these three states and the mechanism of self-association remains. Clearly, as the interconversion of the different states requires a change in pH, CD2d1^{low}, CD2d1^{mid}, and CD2d1^{high} must represent different charge states of the protein that are separated by two protonation equilibria ("pH transitions"), which we equate with pK_a^{low} and pK_a^{high}, as shown in Figure 4.

Concentration Dependence of pH-Induced Variation of Chemical Shifts. We have previously reported that some CD2d1 residues display considerable changes in ^{15}N chemical shifts as a function of protein concentration at pH 6.0 (*16*). These changes can be attributed to the alteration in the chemical environment between the monomeric and dimeric self-associated states on CD2, the populations of which change as a function of protein concentration. With an estimated K_D of 3−6 mM, the proportion of CD2d1 molecules present in the homodimer is estimated to vary between 5 and 30% over the concentration range sampled in the NMR experiments (0.05−1.2 mM) (*16*). We have now extended our chemical shift analysis to probe the effect of pH on main and side chain ^{13}C resonances. The pH titration was performed twice, at protein concentrations of 0.1 and 1.2 mM. By comparison of the titration curves of individual resonances at the two concentrations, it was then possible to separate the effects on the CD2d1 chemical shifts of pH-dependent self-association and protonation equilibria.

The analysis of chemical shift variations was focused on the two pH transitions of Figure 4. Consequently, chemical shift changes were monitored by comparing [^{13}C,^{1}H]-HSQC spectra recorded between pH 3.0 and 5.5 for pK_a^{low} and spectra recorded between pH 5.5 and 8.4 for pK_a^{high}. To simplify the analysis, a threshold was established to define a "significant" absolute chemical shift difference $|\Delta\delta|$ between two pH values as >0.07 ppm. A nucleus with a chemical shift difference of at least this much accumulated in either of the pH ranges, i.e., between pH 3.0 and 5.0 or between pH 5.0 and 8.4, was considered to show an influence of pH. Of 463 carbon resonances assigned at pH 5.0 (*18*), 309 could be followed in two-dimensional (2D) constant-time [^{13}C,^{1}H]-HSQC spectra throughout the pH titration. At a sample concentration of 1.2 mM, more than half of these signals (181) showed a significant pH-dependent ^{13}C chemical shift difference between pH 3.0 and 5.4, with 98 demonstrating a significant ^{13}C chemical shift difference in the high-pH range. The experiment was then repeated at a protein concentration of 0.1 mM. At this lower concentration, a total of 155 resonances yielded a chemical shift difference in the low-pH window and 64 resonances in high-pH window. The greater number of chemical shift differences arising in the high-concentration pH titration is consistent with the model in which the extent of CD2d1 self-association is both pH- and concentration-dependent.

To separate the chemical shift differences resulting from structurally "local" side chain acid−base titration influences from chemical shift differences effected by molecular self-association, the data obtained at high and low protein concentrations were then compared to each other. The difference in the absolute chemical shift difference $\Delta\Delta\delta$ was extracted by subtracting the pH-dependent chemical shift differences for the two protein concentrations for each of the two pH ranges that were considered.

$$\Delta\Delta\delta = |\Delta\delta([\text{CD2d1}] = 1.2\text{ mM})| - |\Delta\delta([\text{CD2d1}] = 0.1\text{ mM})|$$

Again, a threshold for $|\Delta\Delta\delta|$ of >0.07 ppm was adopted to identify all those resonances with a significant pH-dependent chemical shift only at high protein concentrations. Our hypothesis is that these resonances are derived from residues that are located in, and immediately around, the self-association intermolecular interface. For the low-pH range, a total of 37 nuclei were identified in this category, arising from residues I27, R31, W32, E33, R34, G35, T37, L38, V39, E41, L50, K51, T69, V78, T79, Y81, T83, T86, R87, A92, and L93 (using the one-letter code). The 20 residues that have resonances that exhibit a significant chemical shift in the high-pH range are D28, R31, R34, S36, T37, L38, R44, K45, M46, P48, L50, K51, S52, T69, N77, T79, Y81, T86, R87, and I88. These two sets of atoms are depicted separately on the structure of CD2d1 in Figure 5. All carbon atoms that have been shown to demonstrate a pH-dependent chemical shift (between pH 3.0 and 5.0 and between pH 5.0 and 8.4) only at the high protein concentration are indicated in red in the structure of CD2d1. These atoms clearly cluster on the surface of the protein, comprising the major C′−C−F−G β-sheet face which corresponds to the major lattice contact in crystals of the intact CD2 ectodomain. None of the atoms with a significant $\Delta\Delta\delta$ are situated on the opposite side of the protein. That the two sets of residues with significant chemical shifts both strongly populate the same region of the CD2d1 molecule is consistent with the hypothesis that at the extrema of the pH titration the CD2 molecules are tending toward the fully dissociated (monomer) state.

Effects of the E41Q and E29Q Mutations on CD2d1 Dynamics Parameters. It is notable that the residues implicated by these results in the CD2 homodimer interface are clustered around Glu41 (see Figure 5), a residue which we have shown exhibits an anomalously elevated pK_a (*18*), and additional acidic residues, including Asp28, Glu29, and Glu33. A sensible hypothesis is that the protonation equilibrium for Glu41 provides the origin of the high-pH

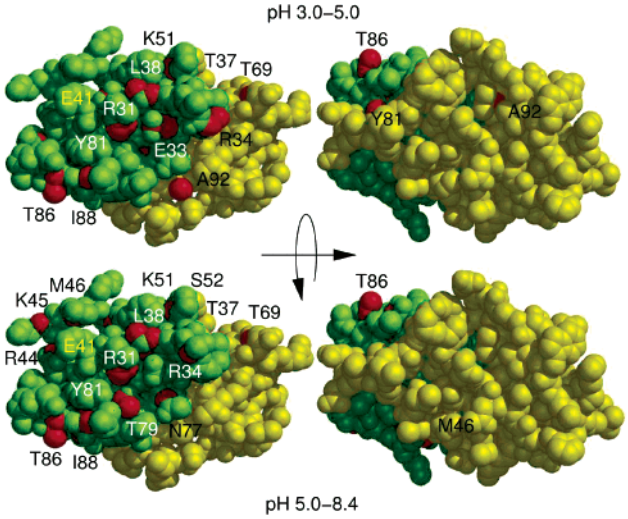

FIGURE 5: Map of pH-dependent carbon chemical shift variations on the structure of rat CD2d1 (from PDB entry 1HNG). The molecule is oriented with the C′−C−F−G β-sheet face facing the front (left) and rotated around 180° around its principal axis (right). Carbon atoms shown in red exhibit a chemical shift variation above the threshold of 0.07 ppm in the indicated pH range. The amino acids in the CD2 ectodomain crystal lattice contact are colored green.

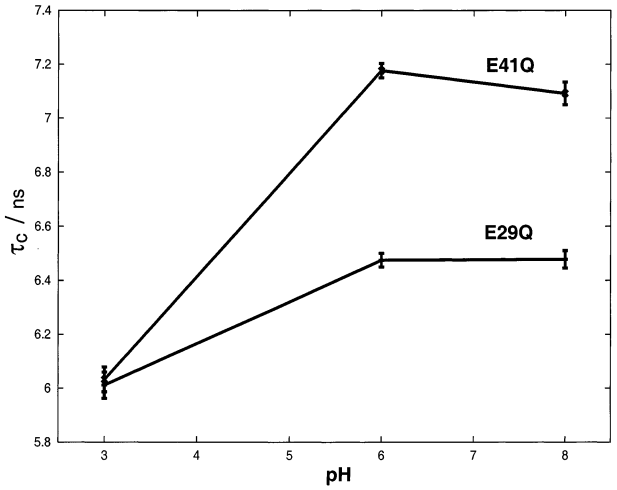

FIGURE 6: Dependence of τ_c on pH for the E29Q and E41Q CD2d1 mutants at 25 °C (^{1}H, 500 MHz).

transition of Figure 4, with perhaps other acidic residues with more standard values of the acidity constant providing the basis for the low-pH transition. On this basis, the CD2d1^{low} state corresponds to molecules with all Glu and Asp residues in their protonated (COOH) form and CD2d1^{high} corresponds to molecules with all Glu and Asp residues in their deprotonated (COO^-) state; CD2d1^{mid} corresponds to molecules in which all Asp and Glu residues are deprotonated except for Glu41 which is in the protonated form.

To test this model, we examined the behavior of mutant forms of CD2d1 in which either Glu29 or Glu41 is substituted with a Gln residue. The isosteric Glu41 → Gln (E41Q) mutant of CD2d1 eliminates the titratable group at this position. Since in the wild type the origin of the elevated pK_a of Glu41 is its proximity to the side chain of Glu29, the isosteric Glu29 → Gln (E29Q) mutant has the effect of both removing the titratable group at the residue 29 position and depressing the pK_a of Glu41 from 6.7 to a more normal value (5.0) (*17*).

^{15}N nuclear relaxation measurements were carried out for both E29Q and E41Q at a protein concentration of 1.2 mM for three pH values (pH 3.0, 6.0, and 8.0). The variations of the sequence-specific profile of the derived order parameters S^2 as a function of pH for the two mutants are essentially the same as for the wild type (data not shown), indicating that the substitutions at residue positions 29 and 41 do not undermine the integrity of the protein fold. The variation of model-free formalism-derived τ_c with pH is depicted in Figure 6. The most striking difference with respect to the wild type is seen for the E29Q mutant. At pH 6.0, the τ_c of the mutant is reduced by more than 1 ns. In addition, the τ_c stays constant at pH >6 and drops only slightly over the pH range of 6−3 (ca. 0.4 ns compared to 1.6 ns for the wild type). The E41Q mutant behaves like E29Q in the high-pH side of the titration by demonstrating only very little variation in τ_c between pH 6.0 and 8.0. However, this mutant has a τ_c close to that of the wild type at pH 6.0, and the value drops almost as quickly as for the wild type when going to acidic pH.

The behavior of these mutants is broadly consistent with the expectation of our hypothesis for the molecular identity of CD2d1^{low}, CD2d1^{mid}, and CD2d1^{high} (Figure 4). Namely, the E41Q mutant which "locks in" the uncharged status of residue 41 retains an elevated τ_c in the middle-pH range, suggesting that self-association of the mutant protein is retained. At low pH, E41Q returns diminished values of τ_c, presumably arising from a lowered level of self-association as the other acidic side chains are protonated. For the E29Q mutant, the pH profile of rotational correlation times is much flatter than for both the wild type and the E41Q mutant. Such behavior is consistent with the removal of the primary cause of the elevated pK_a of Glu41 that confers its special status within the context of the self-association process.

DISCUSSION

pH Dependence of CD2d1 Self-Association. All parameters used in this NMR study [^{13}C chemical shifts, ^{15}N exchange line broadening (R_{ex}), and rotational correlation times (τ_c)] unambiguously point to a strongly pH dependent self-association of CD2d1 which is strongest at pH ≈6.0. A peak in all these parameters implies that self-association is linked to two titration events: one with pK_a^{low} ≈ 4.3 and another with pK_a^{high} ≈ 6.5 (Figure 4). The extensive pH-dependent ^{13}C chemical shift data presented here and large R_{ex} contributions to the ^{15}N resonances of Thr37, Thr79, and other residues (*16*) implicate the C′−C−F−G β-sheet face as the intermolecular interface of the weakly associated CD2 homodimer. We have previously interpreted the concentration-dependent R_{ex} contributions to ^{15}N line widths for wild-type CD2d1 in terms of the model of a CD2 homodimer provided by the major lattice contact in the crystal structure of the intact CD2 ectodomain (*15*), in which the exposed predominantly polar side chains of the C′−C−F−G β-sheet face of one protomer are packed against the corresponding face of another protomer. In addition, the C−C′ loop of one protomer makes backbone H-bond interactions with the F−G loop of the opposing protomer. The interface buries ca. 700 Å^2 of surface area per protomer (*15*). A remarkable aspect of this interface is that it is retained in aberrantly folded forms

of the CD2d1 that give rise to a metastable domain-swapped homodimer under certain conditions of protein expression (*24*, *25*). When these observations are taken as a whole, it seems reasonable to adopt the crystal lattice contact as a model with which to rationalize the solution NMR solution parameters.

We have recently established that Glu41, which resides in the center of the predicted CD2d1 homodimer interaction surface, has an elevated pK_a of 6.7 (*17*), making this residue the prime candidate for the origin of the high-pH transition in the equilibrium of Figure 4. His12, the only other residue with a similar pK_a [the directly measured value is 6.8 (*17*)], can be excluded from consideration as it is on the opposite site of the protein fold and pH chemical shift changes in the neighborhood of His12 are independent of protein concentration as shown in Figure 5 (and the table in the Supporting Information). The assignment of pK_a^{high} to the side chain of Glu41 is reinforced by the weak dependence of the measured value of the pK_a for this residue on protein concentration (*17*), suggesting that the elevated pK_a is in part due to intermolecular interactions at higher protein concentrations. The pattern of altered dynamic properties in the E41Q and E29Q CD2d1 mutants is also consistent with this pK_a assignment. We have shown previously that Glu29's proximity to Glu41 is the major factor contributing to the elevation of the pK_a of the latter residue (*17*). The E29Q mutant has a lower value of τ_c at all pH values (Figure 6), indicating a weakened tendency for dimerization, which is due to the removal of the influence of the Glu29 carboxylate on the pK_a of Glu41.

It is more difficult to specifically assign the pK_a^{low} of Figure 4 to a single residue, though it is within the range that is typically observed for Glu or Asp side chains. Four acidic residues contribute to the putative CD2d1 self-association interface: Asp28, Glu29, Glu33, and Glu41. Of these, Glu41 has already been identified as the origin of pK_a^{high}. The directly measured pK_as of Asp28, Glu29, and Glu33 are 3.57 (3.53), 4.42 (4.39), and 4.16 (4.02) at 1.2 mM (0.1 mM), respectively (*17*), suggesting that the acid−base equilibrium for either or all of these residues has a role in the low-pH transition; in the model, we propose that Asp28, Glu29, and Glu33 must be deprotonated, while Glu41 is still protonated, for CD2d1 self-association to occur. The dual requirement on the protonation states limits self-association to a narrow pH range, consistent with our observations of a peaking of the parameters that characterize the weak interaction.

Mechanism and Dynamics of Self-Association. It is instructive to examine more closely the model for self-association provided by the CD2 crystal lattice contact. The central region of the lattice contact is shown in atomic representation in Figure 7. This picture shows that the side chains of Asp28, Glu29, Arg31, Glu41, and Lys43 from each protomer contribute to the focus of the interface, with Glu33 and Arg87 more on the periphery. To aid clarity, we have also reduced the detailed atomic information contained within the crystal structure to a schematic diagram given in Figure 8 that summarizes the principal features of the C′−C−F−G β-sheet side chain interactions.

When intraprotomer contacts are considered first, it is noteworthy that the closest approach between the side chains

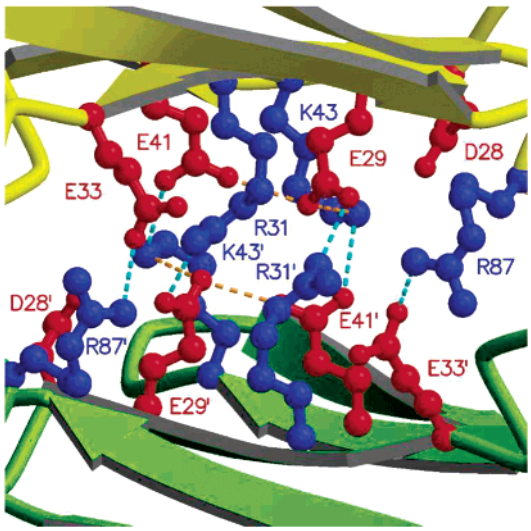

FIGURE 7: Detailed depiction of the interaction of charged residues in the CD2d1 homodimer interface in the crystal lattice contact. Glutamate and aspartate residues are shown in red, and arginine and lysine residues are shown in blue. Distances between the charged groups of these residues short enough for hydrogen bonds or charge−charge interactions are represented with dotted lines in cyan for intermolecular and orange for intramolecular contacts.

of Glu29 and Glu41 is between Glu29 Oϵ1 and Glu41 Oϵ2, a distance (2.92 Å) that is consistent with the formation of a hydrogen bond between the two atoms. In addition, the Oϵ1 atom of Glu29 is in the proximity of the side chain Nζ of Lys43 (2.89 Å), consistent with the presence of a salt bridge H-bond. These observations suggest that Glu29 resides in the deprotonated state within the crystal structure, while Glu41 must be in the protonated state (Oϵ2−H tautomer) to rationalize the predicted intramolecular H-bond with Glu29. The proximity of Glu29 and Glu41 has been used to explain the elevated pK_a of Glu41. The proximity of Lys43 and Glu29 possibly leads to a compensation of the depression of the pK_a of Glu29 that might be predicted on the basis of an isolated interaction between two chemically equivalent titrating groups (*17*). Lys43 Nζ is 2.88 Å from the Oδ2 atom of Asp28, suggesting that these two groups are also in an intramolecular salt bridge H-bond contact.

Examination of the interatomic distances between protomers in the lattice contact suggests the presence of symmetrical salt bridge H-bonds between Arg31 (protomer A/B) and Glu29 (protomer B/A): the separation of Arg31 Nη2 and Glu29 Oϵ2 is just 2.65 Å. The close contact between Arg87 Nη1 and Glu33 Oϵ1 (3.00 Å) suggests another salt bridge H-bond interaction. Intermolecular contacts at slightly greater separation distances are seen between Glu41 Oϵ2 and Glu29 Oϵ1 (3.56 Å) and between Glu41 Oϵ1 and Lys43 Nζ (3.37 Å). Again, the pattern of distances is consistent with a Glu41 side chain protonated on Oϵ2.

Let us consider the likely effect of pH changes upon this lattice contact. The opposing β-sheet faces bring into proximity the following residues for each protomer: basic residues Arg31, Lys43, and Arg87 and acidic residues Asp28, Glu29, Glu33, and Glu41. The acidic residues outnumber the basic residues. It is clear therefore that if all these side chains retained normal acidity constants then the structure of the lattice contact would predict an imbalance of negative charge over positive charge in the pH range above the pK_as of the Asp and Glu residues, and below the pK_as of the basic

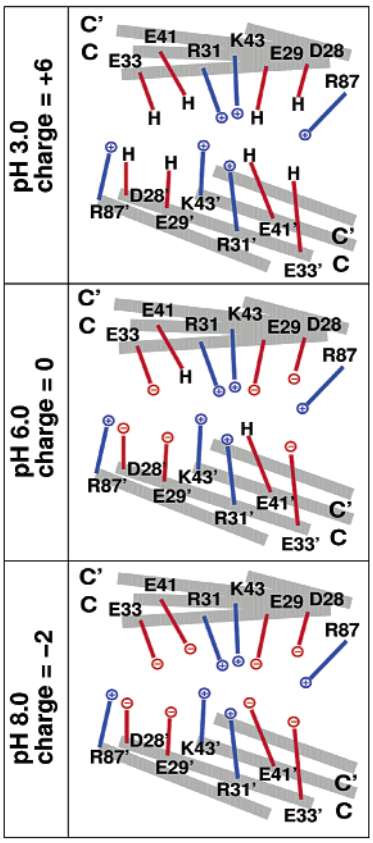

FIGURE 8: Schematic representation of the interactions between rat CD2d1 protomers focusing on the charged residues within the crystal lattice contact between C′−C−F−G β-sheet faces. Two sets of gray bars represent the opposing β-sheets; thin lines indicate the approximate disposition of the side chains (compare with Figure 7). The charge states of the side chains are considered for different pH values: protonated Asp and Glu residues are indicated with H. The overall interfacial charge is indicated in each panel. Only at pH ca. 6.0 is the charge imbalance of the opposing molecular surfaces neutralized.

residues. If the pK_a of Glu41 were a standard value, then the intermolecular interface would have to accommodate an excess of two negative charge units per homodimer at pH ≈6. It is unlikely that under such circumstances the homodimer would be at all stable due to electrostatic repulsion. Rather, it seems that only because of the anomalously high pK_a of Glu41 can the H-bonding network formed in the crystal lattice contact be formed. In this manner, the potential for charge imbalance in the solvent-excluded interface is removed because the side chain of Glu41 remains in the uncharged carboxyl form. Under the terms of this model, both high and low pH values will favor the monomeric species because of the charge imbalance enforced by either protonation of Glu29 and other acid side chains (below pH ≈4.3) or deprotonation of Glu41 (above pH ≈7) (Figure 8).

Taken together, these considerations of the crystal lattice contact fit well with the data obtained on both wild-type and mutant forms of CD2d1. Namely, the model proposed for the pH- and concentration-dependent dynamic and hydrodynamic characteristics in Figure 4 is appropriate for encompassing the observations we have made. We equate pK_a^{high} with the acidity constant for the Glu41 side chain and CD2d1^{mid}, the charge state of CD2d1 that is competent to form weakly associating homodimers, with molecules where all acidic residues are deprotonated except for Glu41.

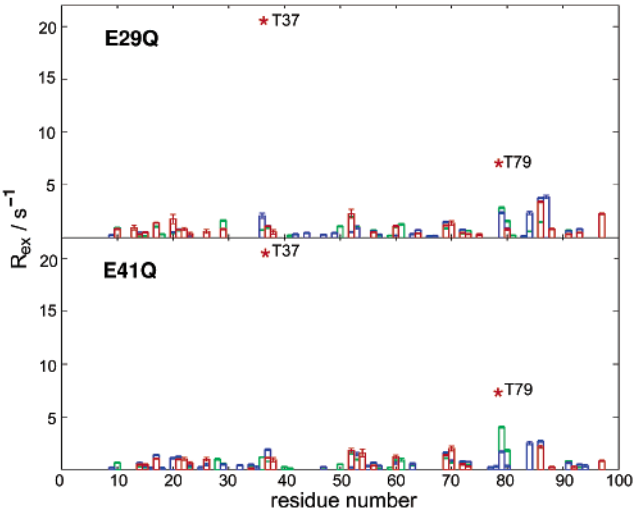

FIGURE 9: Dependence of R_{ex} on pH for the mutants E29Q (top) and E41Q (bottom) at 25 °C (^{1}H, 500 MHz). Values of the exchange value for selected residues in wild-type CD2d1 at pH 6.0 are indicated by red stars. Values for pH 3.0 are shown in green, for pH 6.0 in blue, and for pH 8.0 in red.

We associate pK_a^{low} with the ionizations of other interfacial acidic residues which have been shown to possess more standard values. The structure of the self-associated homodimer in solution is likely to be closely similar to that observed in the lattice contact of the CD2 ectodomain, which we suggest shows the Glu41 side chain in the protonated state.

The detailed nature of this study was in part provoked by the very large values of R_{ex} observed for selected residues in wild-type CD2d1 (*16*). The R_{ex} exchange contributions to R_2 that were detected for CD2d1^{mid} in the case of high concentrations of the wild-type protein are essentially abolished for both mutants (see Figure 9). The only residues that exhibit values of R_{ex} well above 1 s^{-1} correspond to those that did not show a noticeable pH dependence for wild-type CD2d1. Most importantly, in the two mutants R_{ex} of Thr37 never exceeds 3 s^{-1} under any condition that was studied, compared to a maximum R_{ex} value of 22 s^{-1} for this residue in the wild type. As we have shown before, and reinforced in this work, the highlighted wild-type CD2d1 exchange broadening results largely from the self-association of the protein molecules (*16*). The weak affinity of this interaction, provided by the very fast off-rate, combined with the extrapolated chemical shift differences for the monomer and homodimer states is in effect tuned to generate the large R_{ex} contribution that we have observed. We also previously suggested that for Thr37 and Thr79, dimerization might be coupled to alteration of the χ_1 side chain torsion angle in such a manner that the ^{15}N chemical shift differences associated with the dimerization are maximized (*16*). We can only speculate at this stage about why the R_{ex} terms are not so large for the E29Q and E41Q mutants. Using the maximal value of τ_c (Figure 1) as a guide to homodimer affinity, we can estimate that both E29Q and E41Q form homodimers with dissociation constants higher than that of the wild-type. As a consequence, at a given protein concentration and buffer pH, the fraction of homodimer present will be considerably reduced for the mutants compared to the wild type. As indicated in eq 3 of ref *16*, the exchange broadening is maximal at a 1:1 monomer:dimer ratio. Even

if the kinetics of self-association would be identical for the mutants, we would expect the exchange broadening to be markedly reduced.

CONCLUDING REMARKS

In summary, we have completed an in-depth analysis of the concentration- and pH-dependent dynamic and hydrodynamic processes that complicate the ^{15}N relaxation landscape for the T-cell adhesion protein domain rat CD2d1. This contribution, which focuses mainly upon the pH dependence of the rotational correlation time, has reinforced our preliminary conclusion that CD2d1 molecules can self-associate to form a homodimeric structure in solution that possesses the hallmarks of the structure found in related crystal contacts, and metastable misfolded states of the molecule. These data confirm that fine control of pH and protein concentration should be exercised in formulating hypothetical mechanisms for rationalizing R_{ex} exchange contributions to the resonance line width.

Chemical exchange broadening of ^{15}N resonances corresponding to the C′−C−F−G ligand binding face of the homologous human CD2 domain has previously been reported (*9*). This phenomenon was ascribed to multiple conformations fluctuating with millisecond to microsecond motions. However, it is noteworthy that the intact ectodomain of human CD2 crystallizes with a major intermolecular lattice contact that is essentially identical to that observed for rat CD2 (*26*). Namely, for both human and rat CD2, a molecular interface is constructed out of mainly polar residues on the C′, C, F, and G β-strands. It is therefore conceivable that the origin of chemical exchange line broadening for human CD2d1 is again a self-association equilibrium in solution. In this context, it is instructive to consider the relationship between the human and rat CD2 crystal contacts. The rat CD2 crystal contact includes residues Asp28, Glu29, Glu33, Arg31, Glu41 (in its protonated form), Lys43, and Arg87, and the overall charge of these residues is balanced (three negative charges and three positive charges per protomer). The corresponding residues for human CD2 are Asp31, Asp32, Lys34, Glu36, Qln46, Arg48, and Lys82. Interestingly for human CD2, compared to the rat protein, only two of these seven structurally equivalent residues are absolutely conserved. Nevertheless, the overall charge balance is apparently retained. Notably, Gln46 which is equivalent to Glu41, protonated in the rat protein, is not a charged residue.

The physiological role of CD2 is to maintain cell−cell adhesion by forming networked interactions with CD58 (in human) and CD48 (in rodents) on adjacent cells (*27*). The ectodomains of CD2, CD48, and CD58 are highly related molecules in terms of both sequence and three-dimensional structure and have been suggested to derive from a common ancestral gene (*28*, *29*). The structure of the complex of the N-terminal domains of CD2 and CD58 (*30*) revealed a mode of association that is highly reminiscent of the CD2 homodimers presenting both the rat and human CD2 crystal lattices (*15*, *26*). Results from other analyses support a similar model for rat CD2 binding to CD48 (*14*, *31*−*33*). The structure is consistent with the proposal that the crystal lattice contacts present a relic of a more primitive component of a cell−cell adhesion mechanism (*28*). In that we have clearly demonstrated that rat CD2d1 self-associates in solution in a manner similar to the crystal contact (*16*), and that there is conservation of the interfacial charge profile between rat and human CD2 (this work), making it likely that a similar mechanism exists for human CD2, our work would support this view.

Our findings are consistent with previous results which indicate that at physiological pH, the level of homodimeric interaction is low and difficult to detect by other means (*34*). Our results, however, also demonstrate that at lower pH, the propensity for CD2 dimer formation is increased, showing that the binding properties of adhesion molecules can change with pH, and this variation in adhesion properties may have implications for the functioning of adhesion molecules in general. Low pH may be found in the acidic microenvironment of inflamed tissue and growing solid tumor (*35*), and the change in binding behavior of adhesion molecules may therefore have relevance for the change in activity of T-cells at such regions (*34*). Further experiments, however, are required to establish how the change in pH may affect the binding properties and functioning of different receptors in the membrane-bound context in vitro and in vivo.

ACKNOWLEDGMENT

This is a contribution from the Bloomsbury Centre for Structural Biology which is supported by the BBSRC.

SUPPORTING INFORMATION AVAILABLE

Table of pH-dependent ^{13}C chemical shift changes. This material is available free of charge via the Internet at http://pubs.acs.org.

REFERENCES

1. Kay, L. E., Torchia, D. A., and Bax, A. (1989) *Biochemistry 28*, 8972−8979.
2. Palmer, A. G., Williams, J., and McDermott, A. (1996) *J. Phys. Chem. 100*, 13293−13310.
3. Lipari, G., and Szabo, A. (1982) *J. Am. Chem. Soc. 104*, 4546−4559.
4. Lipari, G., and Szabo, A. (1982) *J. Am. Chem. Soc. 104*, 4559−4570.
5. Clore, G. M., Driscoll, P. C., Wingfield, P. T., and Gronenborn, A. M. (1990) *Biochemistry 29*, 7387.
6. Barbato, G., Ikura, M., Kay, L. E., Pastor, R. W., and Bax, A. (1992) *Biochemistry 31*, 5269−5278.
7. Clore, G. M., Szabo, A., Bax, A., Kay, L. E., Driscoll, P. C., and Gronenborn, A. M. (1990) *J. Am. Chem. Soc. 112*, 4989−4991.
8. Banci, L., Felli, I., and Koulougliotis, D. (1998) *J. Biomol. NMR 12*, 307−318.
9. Wyss, D. F., Dayie, K. T., and Wagner, G. (1997) *Protein Sci. 6*, 534−542.
10. Kristensen, S. M., Siegal, G., Davis, B., Sankar, A., and Driscoll, P. C. (2000) *J. Mol. Biol. 299*, 771−788.
11. Wong, K.-G., Fersht, A. R., and Freund, S. M. V. (1997) *J. Mol. Biol. 258*, 494−511.
12. Li, Y.-C., and Montelione, G. T. (1995) *Biochemistry 34*, 2408−2423.
13. Driscoll, P. C., Cyster, J. G., Campbell, I. D., and Williams, A. F. (1991) *Nature 353*, 762−765.
14. McAlister, M. S. B., Mott, H. R., van der Merwe, P. A., Campbell, I. D., Davis, S. J., and Driscoll, P. C. (1996) *Biochemistry 35*, 5982−5991.
15. Jones, E. Y., Davis, S. J., Williams, A. F., Harlos, K., and Stuart, D. I. (1992) *Nature 360*, 232−239.
16. Pfuhl, M., Chen, H. A., Kristensen, S. M., and Driscoll, P. C. (1999) *J. Biomol. NMR 14*, 307−320.
17. Chen, H. A., Pfuhl, M., McAlister, M. S. B., and Driscoll, P. C. (2000) *Biochemistry 39*, 6814−6824.
18. Chen, H. A., Pfuhl, M., Davis, B., and Driscoll, P. C. (1998) *J. Biomol. NMR 12*, 457−458.

19. Vuister, G. W., and Bax, A. (1992) *J. Magn. Reson. 98*, 428−435.
20. Delaglio, F., Gzesiek, S., Vuister, G. W., Zhu, G., Pfeifer, J., and Bax, A. (1995) *J. Biomol. NMR 6*, 277−293.
21. Kraulis, P. J. (1989) *J. Magn. Reson. 24*, 627−633.
22. Boucher, W. (1995) *AZARA*, version 1.0, Department of Biochemistry, University of Cambridge, Cambridge, U.K.
23. Bartels, C., Xia, T.-H., Billeter, M., Güntert, P., and Wüthrich, K. (1995) *J. Biomol. NMR 5*, 1−10.
24. Murray, A. J., Lewis, S. J., Barclay, A. N., and Brady, R. L. (1995) *Proc. Natl. Acad. Sci. U.S.A. 92*, 7337−7341.
25. Hayes, M. V., Sessions, R. B., Brady, R. L., and Clarke, A. R. (1999) *J. Mol. Biol. 285*, 1857−1867.
26. Bodian, D. L., Jones, E. Y., Harlos, K., Stuart, D. I., and Davis, S. J. (1994) *Structure 2*, 755−766.
27. Davis, S. J., and van der Merwe, P. A. (1996) *Immunol. Today 17*, 177−187.
28. Williams, A. F., and Barclay, A. N. (1988) *Annu. Rev. Immunol. 6*, 381−405.
29. Wong, Y. W., Williams, A. F., Kingsmore, S. F., and Seldin, M. F. (1990) *J. Exp. Med. 171*, 2115−2130.
30. Wang, J.-H., Smolyar, A., Tan, K., Liu, J.-H., Kim, M., Sun, Z. J., Wagner, G., and Reinherz, L. (1999) *Cell 97*, 37−45.
31. van der Merwe, P. A., McNamee, P. N., Davies, E. A., Barclay, A. N., and Davis, S. J. (1995) *Curr. Biol. 5*, 74−84.
32. Davis, S. J., Davies, E. A., Tucknott, M. G., Jones, E. Y., and van der Merwe, P. A. (1998) *Proc. Natl. Acad. Sci. U.S.A. 95*, 5490−5494.
33. Davis, S. J., Ikemizu, S., Wild, M. K., and van der Merwe, P. A. (1998) *Immunol. Rev. 163*, 217−236.
34. Zhu, B., Davies, E. A., van der Merwe, P. A., Calvert, T., and Leckband, D. E. (2002) *Biochemistry 41*, 12163−12170.
35. Martin, G. R., and Jain, R. K. (1994) *Cancer Res. 54*, 5670−5674.

BI026447X